Semiquantitative ^{123}I-Metaiodobenzylguanidine Scintigraphy to Distinguish Pheochromocytoma and Paraganglioma from Physiologic Adrenal Uptake and Its Correlation with Genotype-Dependent Expression of Catecholamine Transporters

Anouk van Berkel[1], Jyotsna U. Rao[1], Jacques W.M. Lenders[2,3], Natalia S. Pellegata[4], Benno Kusters[5,6], Ianthe Piscaer[1], Ad R.M.M. Hermus[1], Theo S. Plantinga[1], Johan F. Langenhuijsen[7], Dennis Vriens[8], Marcel J.R. Janssen[8], Martin Gotthardt[8], and Henri J.L.M. Timmers[1]

[1]Division of Endocrinology, Department of Internal Medicine, Radboud University Medical Centre, Nijmegen, The Netherlands; [2]Division of Vascular Medicine, Department of Internal Medicine, Radboud University Medical Centre, Nijmegen, The Netherlands; [3]Department of Internal Medicine III, University Hospital Carl Gustav Carus, Technical University Dresden, Dresden, Germany; [4]Institute of Pathology, Helmholtz Zentrum München-German Research Center for Environmental Health, Neuherberg, Germany; [5]Department of Pathology, Radboud University Medical Centre, Nijmegen, The Netherlands; [6]Department of Pathology, Maastricht University Medical Centre, Maastricht, The Netherlands; [7]Department of Urology, Radboud University Medical Centre, Nijmegen, The Netherlands; and [8]Department of Radiology and Nuclear Medicine, Radboud University Medical Centre, Nijmegen, The Netherlands

^{123}I-metaiodobenzylguanidine (^{123}I-MIBG) scintigraphy plays an important role in the diagnostic evaluation of patients with pheochromocytoma and paraganglioma (PPGL). ^{123}I-MIBG targets cell membrane and vesicular catecholamine transporters of chromaffin cells and facilitates localization of the primary tumor and metastatic lesions. Its specificity for the diagnosis of adrenomedullary chromaffin cell tumors can be jeopardized by physiologic uptake by the normal adrenal medulla. The aim of this study was to distinguish between PPGLs and normal adrenal glands by evaluating semiquantitative ^{123}I-MIBG uptake and to examine genotype-specific differences in correlation with expression of catecholamine transporter systems. **Methods:** Sixty-two PPGLs collected from 57 patients with hereditary mutations in *SDHA* ($n = 1$), *SDHB* ($n = 2$), and *SDHD* ($n = 4$) (*SDH* is succinate dehydrogenase); von Hippel-Lindau (*VHL*; $n = 2$); *RET* ($n = 12$); neurofibromin 1 (*NF1*; $n = 2$); and MYC-associated factor X (*MAX*; $n = 1$), and with sporadic PPGLs ($n = 33$) were investigated. Preoperative planar and SPECT images were semiquantitatively analyzed using uptake measurements. Tumor-to-liver and normal adrenal–to–liver ratios were calculated and correlated with clinical characteristics including genotype, tumor size, and plasma metanephrines concentrations. The expression of norepinephrine transporter (NET) and vesicular monoamine transporter (VMAT-1) was evaluated immunohistochemically in paraffin-embedded tumor tissues. **Results:** Mean tumor-to-liver ratios of PPGL lesions were significantly higher than normal adrenal–to–liver ratios ($P < 0.001$). Cutoff values to distinguish between physiologic and pathologic adrenal uptake were established at 0.7 (100% sensitivity, 10.3% specificity) and 4.3 (100% specificity, 66.1% sensitivity). No statistically significant differences in ^{123}I-MIBG uptake were found across PPGLs of different genotypes. Mean NET expression in hereditary cluster 2 (*RET, NF1, MAX*) and apparently sporadic tumors was significantly higher than for hereditary cluster 1 (*SDHx, VHL*) PPGLs ($P = 0.011$ and 0.006, respectively). Mean VMAT-1 expression in hereditary cluster 1 PPGLs was significantly higher than for cluster 2 tumors ($P = 0.010$). ^{123}I-MIBG uptake significantly correlated with maximum tumor diameter ($P = 0.002$). ^{123}I-MIBG uptake, however, did not correlate with either NET or VMAT-1 expression. **Conclusion:** Liver-normalized semiquantitative ^{123}I-MIBG uptake may be helpful to distinguish between pheochromocytoma and physiologic adrenal uptake. Genotype-specific differences in the expression of NET and VMAT-1 do not translate into differences in ^{123}I-MIBG uptake.

Key Words: pheochromocytoma; paraganglioma; ^{123}I-metaiodobenzylguanidine; scintigraphy; norepinephrine transporter; vesicular monoamine transporter 1

J Nucl Med 2015; 56:839–846
DOI: 10.2967/jnumed.115.154815

Metaiodobenzylguanidine (MIBG) is a structural and functional analog of norepinephrine that selectively accumulates in noradrenergic neurosecretory granules of sympathetic neurons, ganglia, and chromaffin cells (*1*). Active cellular uptake of MIBG is mediated by the norepinephrine transporter (NET). Intracellularly, MIBG is stored in neurosecretory granules through the action of vesicular monoamine transporters (VMATs) (*2,3*). MIBG has proven to be useful for scintigraphic imaging of pheochromocytomas and paragangliomas (PPGLs) (*4,5*). These rare and often benign catecholamine-producing tumors arise from the adrenal medulla and extraadrenal sympathetic chromaffin tissues (*5*). PPGLs can occur sporadically or in the context of hereditary syndromes (~34%) (*6*). The major susceptibility genes for PPGLs

Received Jan. 23, 2015; revision accepted Mar. 25, 2015.
For correspondence or reprints contact: Henri J.L.M. Timmers, Radboud University Medical Centre, Department of Internal Medicine, Division of Endocrinology 471, P.O. Box 9101, 6500 HB Nijmegen, The Netherlands.
E-mail: Henri.Timmers@radboudumc.nl
Published online Apr. 16, 2015.

include those encoding succinate dehydrogenase (*SDH*) complex subunits and cofactor 2 (*SDHA/B/C/D/AF2*, abbreviated *SDHx*), von Hippel-Lindau (*VHL*), *RET,* neurofibromin 1 (*NF1*), MYC-associated factor X (*MAX*), transmembrane protein 127 (*TMEM127*), and more recently discovered fumarate hydratase (*FH*) and hypoxia-inducible factor-2α (*HIF2A*) (*7,8*). Furthermore, somatic mutations of mainly *NF1* and *VHL* can be detected in up to 30% of sporadic PPGLs (*8*). Hereditary PPGLs have been divided into 2 clusters based on their transcriptional signature (*9,10*). Cluster 1 includes *SDHx-, VHL-, FH-,* and *HIF2A*-related tumors and is characterized by a hypoxia/angiogenesis signature. Cluster 2 includes *NF1-, RET-, MAX-,* and *TMEM127*-related tumors and is associated with the activation of MAP kinase/AKT/mTOR pathways.

At present, scintigraphy with ^{123}I-MIBG is the most commonly used functional imaging technique for localizing PPGLs because of its high specificity and worldwide availability (*4,5*). Its whole-body exploration makes it particularly useful for the evaluation of multifocality and metastatic and recurrent disease. ^{123}I-MIBG is chosen over ^{131}I-MIBG because of higher diagnostic sensitivity, shorter half-life, favorable dosimetry, and improved imaging quality (*11,12*). Besides conventional planar imaging, SPECT imaging provides 3-dimensional information, which can be fused with computerized tomography (SPECT/CT) for anatomic correlation (*13*). Overall, specificities of ^{123}I-MIBG scintigraphy range between 70% and 100% for pheochromocytomas and 84% and 100% for paragangliomas, whereas sensitivities range between 85% and 88% and 56% and 76%, respectively (*14–17*). Physiologic uptake of ^{123}I-MIBG by normal adrenal glands can give false-positive results or obscure small lesions (*18–20*). The sensitivity appears to be lower for extraadrenal, metastatic, recurrent, and certain hereditary PPGLs (*14,16,21–24*). Metastatic lesions might be missed because of cell dedifferentiation and, consequently, loss of NET or VMAT expression. It has been demonstrated that sensitivity was especially low in *SDHB-* and *VHL*-related PPGLs (*22,25,26*). Theoretically, the amount of uptake and, consequently, tumor visualization and susceptibility for ^{131}I-MIBG therapy might be dependent of the underlying genotype.

The aim of this study was to semiquantitatively evaluate ^{123}I-MIBG uptake in PPGLs and to determine whether this uptake can be used to differentiate between pathologic and physiologic adrenal uptake and to distinguish between PPGLs with different underlying genotypes. Therefore, planar and SPECT images were analyzed using automated measurements. Results were correlated with patient clinical characteristics. Additionally, the immunohistochemical expression of NET and VMAT-1 was directly correlated with in vivo ^{123}I-MIBG uptake in PPGLs of different genotypes.

MATERIALS AND METHODS

Patient Population

This study retrospectively included 57 patients (23 males, 34 females; mean age, 44.2 y; age range, 8–71 y) who consecutively underwent preoperative diagnostic ^{123}I-MIBG scintigraphy between October 2002 and February 2014. All patients had suspected PPGL and were referred to the Radboud University Medical Centre. In all cases, the diagnosis of PPGL was confirmed histologically. Fifty-four patients had 58 nonmetastatic PPGLs (49 adrenal, 9 extraadrenal). Four patients had metastatic PPGL, including 1 with paravertebral thoracal lymph node, 2 with paraaortal lymph node, and 1 with retrocaval lymph node metastasis. The presence of germline mutations and large deletions in *SDHA/B/C/D/AF2, RET, VHL, TMEM127, and MAX* was investigated using standard procedures in all patients. Twenty-four patients had an underlying mutation (1 with *SDHA* mutation, 2 with *SDHB* mutation, 4 with *SDHD* mutation, 2 with *VHL* mutation, 12 with *RET*-related multiple endocrine neoplasia type II, 1 with *MAX* mutation, and 2 with *NF1* mutation). In the remaining patients, no genetic alterations were detected in the above-mentioned genes. Their tumors were classified as apparently sporadic. Patients' clinical characteristics and genotype are listed in Table 1 and Supplemental Table 1 (supplemental materials are available at http://jnm.snmjournals.org). All patients underwent biochemical testing before and after surgery. Plasma concentrations of metanephrines (sum of normetanephrine and metanephrine) were assayed using high-performance liquid chromatography (*27*). Tumor sizes were retrieved from pathology reports, and for each PPGL the maximum tumor diameter in centimeters was recorded. Data were collected under conditions of regular clinical care, with the approval of the ethics committee obtained for the retrospective use of those data, for scientific purposes.

Imaging Procedures

Patients received thyroid blockade with a saturated solution of potassium iodide before ^{123}I-MIBG scintigraphy (100 mg/day starting 1 day before tracer injection and continuing for 2 days). Whole-body planar and tomographic (SPECT) images were obtained 24 h after

TABLE 1
Patient Characteristics

Genotype	No. of patients	Sex (M/F)	Age (y)	Tumor location (adrenal/extraadrenal)	Maximum tumor diameter (cm)
Sporadic	33	10/23	45.0 ± 14.8	30/4	5.2 ± 2.9
SDHA	1	0/1	19.0	1/0	8.0
SDHB	2	1/1	30.0 ± 22.6	0/2	5.7 ± 1.0
SDHD	4	2/2	44.0 ± 16.2	1/4	3.4 ± 1.2
VHL	2	1/1	24.0 ± 13.9	1/2	2.2 ± 0.6
Multiple endocrine neoplasia type II	12	8/4	49.0 ± 12.1	14/0	3.8 ± 2.4
NF1	2	0/2	48.0 ± 15.6	1/1	5.3 ± 2.4
MAX	1	1/0	57.0	1/0	1.8

Study included 57 patients with 62 PPGLs. Data are expressed as mean ± SD.

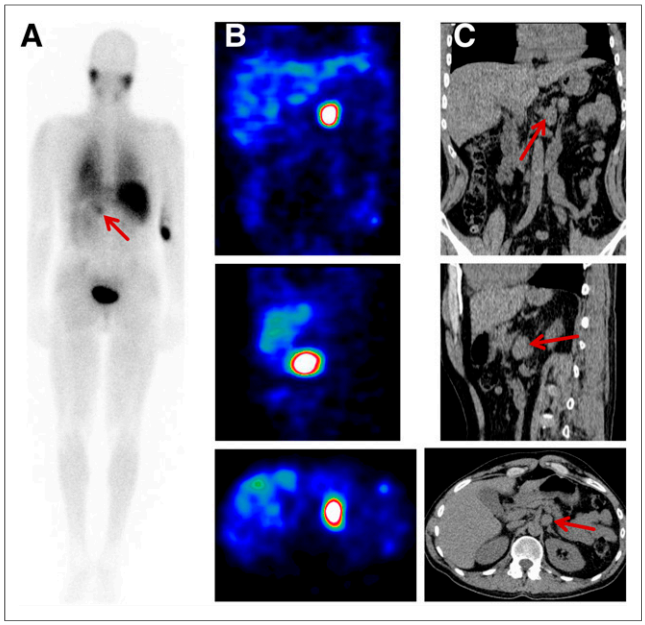

FIGURE 1. ^{123}I-MIBG scintigraphy scans of 50-y-old male patient with *RET* mutation and pheochromocytoma on left side (indicated by arrow). (A) Planar-whole-body scan. (B) SPECT scan. (C) CT scan.

intravenous administration of 302 ± 67 MBq of ^{123}I-MIBG (Fig. 1). Medication with potential interference with ^{123}I-MIBG uptake (*28,29*) was not discontinued in 11 patients for blood pressure safety reasons (Supplemental Table 1).

Of sixty-two ^{123}I-MIBG scans, 39 were obtained before November 2011, using an ECAM (Siemens Healthcare) dual-head γ camera. After November 2011, a Symbia-T16 (Siemens Healthcare) dual-head γ camera was used (22 scans), and SPECT was combined with low-dose CT for anatomic coregistration. One scan was obtained using an Infinia (GE Healthcare) dual-head γ camera. Both Siemens scanners were equipped with a medium-energy low-penetration parallel-hole collimator and calibrated in accordance with the European Association of Nuclear Medicine guidelines for ^{123}I-MIBG scintigraphy (*28*). The acquisition matrix size was 128 × 128. The whole-body scans were acquired from feet to head (8 cm/min continuous bed movement). SPECT imaging was performed with 64 projections per camera head (128 views, sampling angle 2.8°) and an acquisition time of 30 s (ECAM) or 24 s (Symbia T-16) per projection using body-contour orbit (step-and-shoot). During image acquisition, energy windows were centered at 159 keV (photo peak window) and 135 keV (lower scatter window), with a window width of 15%. CT imaging for SPECT/CT was performed without contrast, and the x-ray tube peak voltage (kVp) was set to 110 kV and the x-ray tube current was modulated using CARE Dose4D, with a reference tube current of 50 mAs.

SPECT images were reconstructed using an iterative ordered-subset expectation algorithm as implemented in ReSPECT 2.5 (Scivis wissenschaftliche Bildverarbeitung) with 6 iterations and 32 subsets. Scatter correction was performed using a background subtraction method. In this approach, a body contour detection is used to estimate contribution of background scatter, which is subsequently subtracted from the image. Furthermore, homogeneous attenuation correction is performed during image reconstruction using a semiautomatic body contour detection (Chang's attenuation correction) with a linear attenuation coefficient (μ) of 0.14 cm^{-1} because measured attenuation correction is not implemented in this version of ReSPECT. Postreconstruction filtering was performed with a 3-dimensional gaussian filter kernel with a full width at half maximum of 40 mm. The reconstruction matrix size was 128 × 128 voxels, with an isotropic voxel size of 4.80 mm in all 3 orthogonal directions.

Image Interpretation

Scintigraphic images were retrospectively analyzed, and ^{123}I-MIBG uptake was assessed in adrenal and extraadrenal lesions on SPECT and, if available, planar images. For the nonmetastatic cases, lesions were identified as PPGL in the case of histologic evidence and normalization of plasma metanephrines after surgery. In the case of right adrenal or extraadrenal PPGL, ^{123}I-MIBG uptake was also assessed in the normal left adrenal gland. Normal right adrenal glands were not evaluated because of the difficulty separating them from physiologic uptake by the liver.

SPECT images were reviewed using 2 different software systems: Inveon Research Workplace (IRW) 4.1 (Preclinical Solutions, Siemens Medical Solutions USA) and Hermes 4.6-A (Hermes Medical Solutions AB). Planar images were reviewed only with the latter. Uptake of ^{123}I-MIBG in PPGLs was quantified in relation to hepatic uptake. On SPECT images, lesions were segmented using a relative threshold region-growing algorithm. The seed point for the algorithm was the maximum-intensity voxel, and the segmentation threshold was 70% of the maximum activity concentration within the lesion to eliminate areas with tumor necrosis. A 125-cm^3 cubic or spheric volume of interest was positioned centrally in the patient's upper right liver lobe. In the case of liver involvement, unaffected regions were visually identified. Tumor-to-liver (T/L) ratios were calculated as the mean counts per pixel in the segmented tumor volume of interest over the mean counts per pixel in the liver volume of interest. Likewise, ^{123}I-MIBG uptake in normal left adrenals was quantified, resulting in normal adrenal–to–liver (NA/L) ratios. On posterior planar images, PPGLs were visually delineated, and a region of interest was manually drawn around the tumor. A circular region of interest of 5-cm diameter was positioned centrally in the right upper liver lobe, and T/L ratios were calculated.

Immunohistochemistry for NET and VMAT-1 Protein Expression

Tumor tissue sections (4 μm) were deparaffinized, rehydrated, and washed with 50 mM phosphate-buffered saline (PBS). Immunohistochemistry for NET was performed using an automated immunostainer (Ventana Medical Systems) as previously reported (*30*). The primary antibody directed against NET (clone 05-2 [Mab Technologies]; dilution, 1:500) was diluted in REAL antibody diluent (Dako). The SuperSensitive immunohistochemistry detection system from BioGenex was used to visualize the antibody binding, and the immunoreaction was developed in the diaminobenzidine supplied with the kit (Vector Laboratories). Sections were counterstained with Mayer Haemalum (Roche), dehydrated, and covered with glass coverslips. Sections of normal adrenal gland were used as positive control and included in each run. Sections incubated without the primary antibody were included in each batch as a negative control.

Immunohistochemistry for VMAT-1 was performed manually according to the following protocol. Endogenous peroxidase activity was blocked with 30% hydrogen peroxide (H_2O_2) in PBS for 30 min. Antigen retrieval was performed by boiling the sections in 10 mM sodium citrate, pH 6.0, in a microwave for 2 h 20 min at 800 W, followed by 10 min at 160 W. Sections were cooled at room temperature for 90 min. Before incubation with the primary antibody, endogenous avidin and biotin was blocked (Sp-2001; Vector Laboratories). Nonspecific interactions were blocked using normal goat serum (20% in PBS/1% bovine serum albumin) for 10 min. Slides were incubated with the primary antibody VMAT-1 (H-V001; Phoenix Pharmaceuticals) at a 1:500 dilution overnight at 4°C. The sections were then

washed with PBS, followed by incubation with a secondary biotinylated goat-antirabbit antibody (Vector Laboratories) at a 1:200 dilution for 30 min at room temperature. Slides were subsequently incubated with avidin-biotin reagent (PK6100 Vectastain Elite ABC Kit; Vector Laboratories) for 30 min. The sections were washed with PBS and incubated with 3,3-diaminobenzidine (BS04-110; Immunologic) for 3 min. After being rinsed with running tap water for 5 min, the sections were counterstained with hematoxylin for 1 h 30 min, washed, dehydrated in an ethanol series (50%, 70%, 100%) followed by xylene, and mounted with Permount (ThermoFisher Scientific).

All staining results were assessed by an experienced pathologist who was masked to patients' clinical data. The presence of VMAT-1 and NET tumor cell cytoplasmic staining was graded by the percentage of tumor cells with positive staining. The intensity of staining was categorized as none (0), weak staining (1+), medium staining (2+), and intense staining (3+), ignoring staining of sustentacular cells, which was frequently noted for both proteins. Areas containing adrenal cortex and endothelial cells were used as controls for comparison between different sections. The immunohistochemistry staining score represents the expression of the proteins and was calculated by multiplication of both grades (% positive × intensity).

Statistical Analysis

Normally distributed variables are expressed as mean ± SD. Variables not obeying the normal distribution are described by median and interquartile range (IQR). Calculated uptake ratios from SPECT images reviewed in IRW were used for data analysis. Results were validated against analysis of planar and SPECT images in Hermes using the Spearman rank correlation (ρ) and calculating Bland–Altman limits of agreement (*31*). Cutoff values for pathologic ^{123}I-MIBG uptake were determined using receiver-operating-characteristic curve analysis, and the area under the curve was calculated. Nonparametric tests (Mann–Whitney *U*) were used to compare difference in ^{123}I-MIBG uptake between PPGLs with different location and normal adrenal glands. For comparisons of ^{123}I-MIBG uptake across different genotypes, calculated uptake ratios were analyzed using the independent-samples Kruskal–Wallis test with Dunn posttest. To test for differences in immunohistochemical staining scores for NET and VMAT-1 among different hereditary clusters, the Mann–Whitney *U* test was used. Spearman rank correlations were used to estimate relation between ^{123}I-MIBG uptake, NET and VMAT-1 protein expression, tumor size, and concentrations of plasma metanephrines. Overall, a two-sided *P* value below 0.05 was considered statistically significant. Statistical analyses were performed using SPSS 20.0 statistical software (SPSS Inc.).

RESULTS

Agreement Between Different Methods for Assessing ^{123}I-MIBG Uptake in PPGLs

Calculated T/L ratios of SPECT images in Hermes and IRW were highly correlated ($\rho = 0.995$, $P < 0.001$, Supplemental Fig. 1A) with narrow Bland–Altman limits of agreement (−0.92 to 1.15, Supplemental Fig. 1B). In the Bland–Altman plot, the mean difference line overlapped the line of equality, indicating that Hermes provided T/L ratios similar to IRW (Supplemental Fig. 1B). Furthermore, T/L ratios of planar images, reviewed in Hermes, significantly correlated with T/L ratios of SPECT images reviewed in Hermes ($\rho = 0.582$, $P < 0.001$) and IRW ($\rho = 0.588$, $P < 0.001$).

^{123}I-MIBG Uptake in PPGLs Versus Normal Adrenal Glands

Median T/L ratios of PPGLs were 5.5 (IQR, 3.1–9.5) and significantly higher than NA/L ratios of normal left adrenal glands (median, 1.5; IQR, 0.9–2.3; $P < 0.001$; Fig. 2). T/L ratios of extraadrenal PPGLs were significantly higher than ratios of adrenal PPGLs (median, 8.4; IQR, 6.0–11.1 vs. 5.4; IQR, 2.9–7.3; $P < 0.05$; Fig. 2). Tumor necrosis was visually observed in 3 adrenal and 4 extraadrenal PPGLs, and T/L ratios were similar to nonnecrotic tumors (data not shown). The median T/L ratio of the 11 patients using potentially interfering medication was 3.7 (IQR, 2.0–6.7), whereas that of the 46 patients without those drugs was 5.8 (IQR, 3.1–9.6; $P = 0.164$).

A receiver-operating-characteristic curve was constructed from T/L ratios of extraadrenal PPGLs and NA/L ratios of normal left adrenal glands (area under the curve, 0.916; 95% confidence interval, 0.86–0.97; Fig. 3). To provide 100% sensitivity, the upper reference for physiologic adrenal ^{123}I-MIBG uptake was established at 0.7, resulting in a specificity of 10.3%. To provide 100% specificity, the upper reference for physiologic adrenal ^{123}I-MIBG uptake was established at 4.3 (the maximum value for PPGL-negative normal adrenals), resulting in a sensitivity of 66.1%.

Distribution of ^{123}I-MIBG Uptake Across Different Genotypes

The distribution of T/L ratios in PPGLs across hereditary and apparently sporadic tumors is shown in Figure 4. The median T/L ratio for hereditary cluster 1 tumors (*SDHx, VHL*) was 6.2 (IQR, 5.0–8.1), for hereditary cluster 2 (*RET, NF1, MAX*) 5.4 (IQR, 3.8–8.2), and apparently sporadic tumors 5.8 (IQR, 2.5–10.9). No statistical differences in ^{123}I-MIBG uptake were found between these groups.

The maximum tumor diameter ranged from 0.6 to 14.0 cm (median, 4.1; IQR, 2.5–6.2). ^{123}I-MIBG uptake was positively correlated with maximum tumor diameter in both adrenal and extraadrenal PPGLs ($\rho = 0.380$, $P = 0.002$). The 5 smallest PPGLs, each measuring less than 2.0 cm, all showed uptake of ^{123}I-MIBG with T/L ratios higher than 1.0 (Supplemental Table 1). Furthermore, no statistically significant correlation was found between ^{123}I-MIBG uptake and concentrations of plasma metanephrines ($\rho = 0.229$, $P = 0.076$).

Evaluation of NET and VMAT-1 Protein Expression in PPGLs

Of 62 PPGLs, 61 samples were available for NET staining. Tumor cells in all samples showed a positive cytoplasmic staining

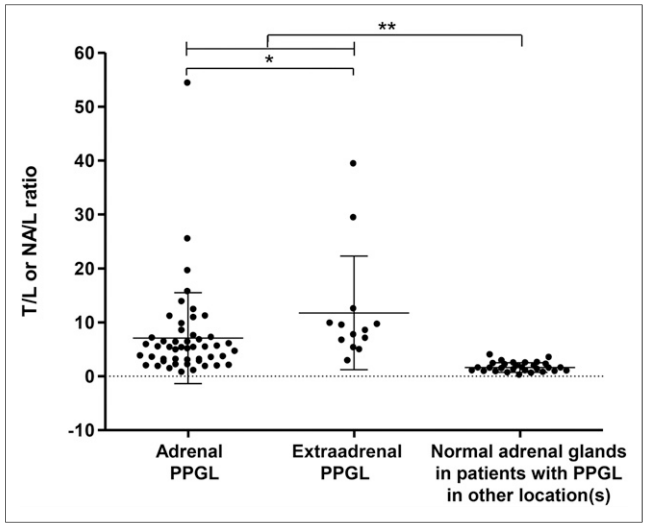

FIGURE 2. ^{123}I-MIBG SPECT uptake expressed as T/L ratio in PPGLs according to tumor location. Uptake in normal adrenals is expressed as NA/L ratio. All ratios are corrected for injected dose and decay. Horizontal bar represents the mean and error bars the SD. *$P < 0.01$, Mann–Whitney *U* test. **$P < 0.01$, Mann–Whitney *U* test.

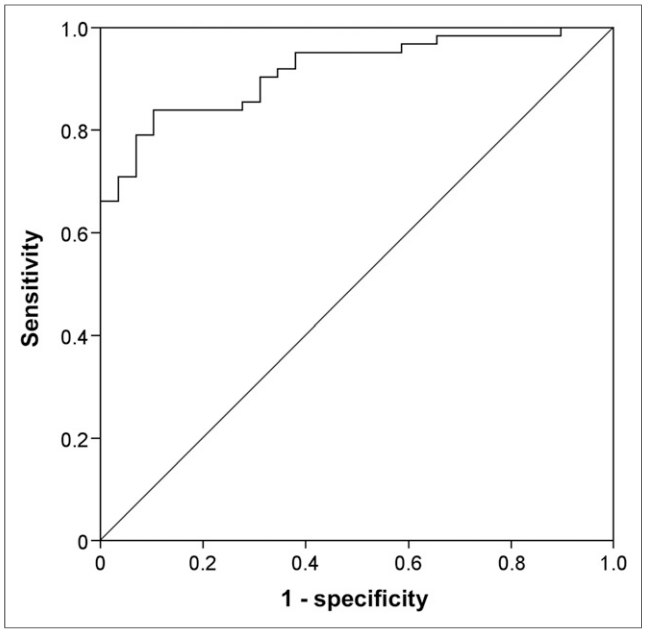

FIGURE 3. Receiver-operating-characteristic curve for ^{123}I-MIBG uptake values. This curve was constructed from T/L ratios of PPGL lesions and NA/L ratios of normal adrenals in patients with PPGL. Diagonal line represents line of no discrimination

for NET, and a clear variability in staining intensity among samples was observed (Fig. 5). Figure 6A shows NET immunohistochemical staining intensity according to genotype. Negative to occasionally weak cytoplasmic staining was encountered in *VHL*- and *MAX*-related PPGLs. The expression of NET in hereditary cluster 2 (*RET, NF1, MAX*) and apparently sporadic tumors was higher than for hereditary cluster 1 (*SDHx, VHL*) PPGLs (108.1 ± 18.7, 94.4 ± 10.9 vs. 41.3 ± 18.4, $P \leq 0.05$, $P \leq 0.01$, Fig. 6A). No statistically significant differences in NET staining were found between cluster 2 and apparently sporadic PPGLs ($P = 0.354$, Fig. 6A).

PPGLs showed cytoplasmic immunoreactivity with the anti–VMAT-1 antibody, and occasionally also sustentacular cells stained positive (Fig. 5). *VHL-, RET-,* and *MAX*-related tumors showed an overall similar VMAT-1 expression, which was usually scored as medium. A highly heterogeneous expression of VMAT-1 was encountered in sporadic PPGLs (Fig. 6B). VMAT-1 expression in hereditary cluster 1 (*SDHx, VHL*) PPGLs was higher than in hereditary cluster 2 (*RET, NF1, MAX*) tumors (193.8 ± 19.1 vs. 135.8 ± 12.3, $P < 0.01$). No significant differences were observed between hereditary and sporadic samples (160.6 ± 11.9 vs. 168.7 ± 12.5, $P = 0.197$, Fig. 6B). Neither NET nor VMAT-1 protein expression correlated with ^{123}I-MIBG uptake ($\rho = -0.103$, $P = 0.203$; $\rho = 0.046$, $P = 0.723$, respectively).

DISCUSSION

Our study provides the first, to our knowledge, semiquantitative analysis of ^{123}I-MIBG scintigraphy in patients with PPGL. Uptake of ^{123}I-MIBG in PPGLs was significantly higher than in normal adrenal glands, and cutoff values were established to distinguish between pathologic and physiologic uptake. The uptake of ^{123}I-MIBG significantly correlated with maximum tumor diameter. No significant differences in ^{123}I-MIBG uptake were found between PPGLs of various genotypic clusters. NET expression was significantly higher in cluster 2 (*RET, NF1, MAX*) and in apparently sporadic PPGLs than in cluster 1 (*SDHx, VHL*) PPGLs. VMAT-1 expression was significantly higher in cluster 1 than cluster 2 tumors. MIBG uptake, however, did not correlate with either NET or VMAT-1 expression.

Traditionally, ^{123}I-MIBG scintigraphy is considered as nonquantitative because of a relatively low tumor-to-background ratio and limited spatial resolution. Scintigraphic image interpretation can be difficult in the case of small lesions and physiologic uptake of ^{123}I-MIBG by normal adrenal glands, which is observed in 50%–80% of cases. Cecchin et al. (*32*) proposed a scoring system in which ^{123}I-MIBG uptake in adrenal glands was visually compared with hepatic uptake. Scintigraphic images were classified as positive in the case of adrenal uptake more intense than in the liver or nonhomogeneous uptake in an enlarged adrenal gland or an extraadrenal focus. They demonstrated that the scoring system was highly specific and sensitive (91.5% and 100%, respectively) for detecting PPGL and is useful to discriminate normal adrenal ^{123}I-MIBG uptake from pheochromocytoma. Others have adopted this approach (*19,23,33*). However, a major disadvantage is that visual interpretation remains subjective and is highly observer-dependent. Thus, assessments of ^{123}I-MIBG uptake may be facilitated using semiquantitative measurement methods. Our present study demonstrates that semiquantitative analysis of ^{123}I-MIBG images can be used for uptake measurements and facilitates the discrimination between adrenal PPGL and physiologic adrenal uptake. Nevertheless, there was considerable overlap between tumoral uptake and physiologic uptake by normal adrenals, and this overlap might still lead to false-negative results, as also observed by Cecchin et al. (*32*). Also, T/L ratios provide a semiquantitative uptake parameter. Actual quantification would require quantitative SPECT using accurately calibrated SPECT reconstructions.

Mechanisms of uptake and storage of ^{123}I-MIBG in sympathetic chromaffin cells is similar to that of norepinephrine. At the cellular membrane level, uptake is mediated by NET (solute carrier family 6 member 2, SLC6A2), a monoamine transporter, which is responsible for the regulation of extracellular norepinephrine levels by active reuptake mechanisms after their release from neuronal or endocrine stores. NET is typically expressed in noradrenergic

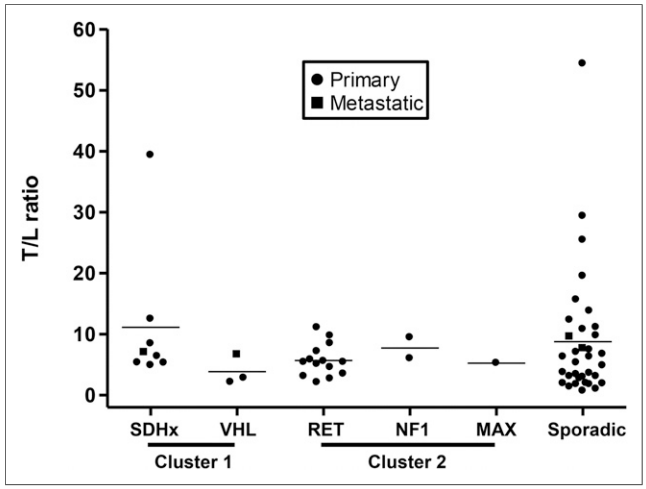

FIGURE 4. ^{123}I-MIBG uptake expressed as T/L ratio in PPGLs across different genotypes. SPECT images analyzed in IRW. All T/L ratios are corrected for injected dose and decay.

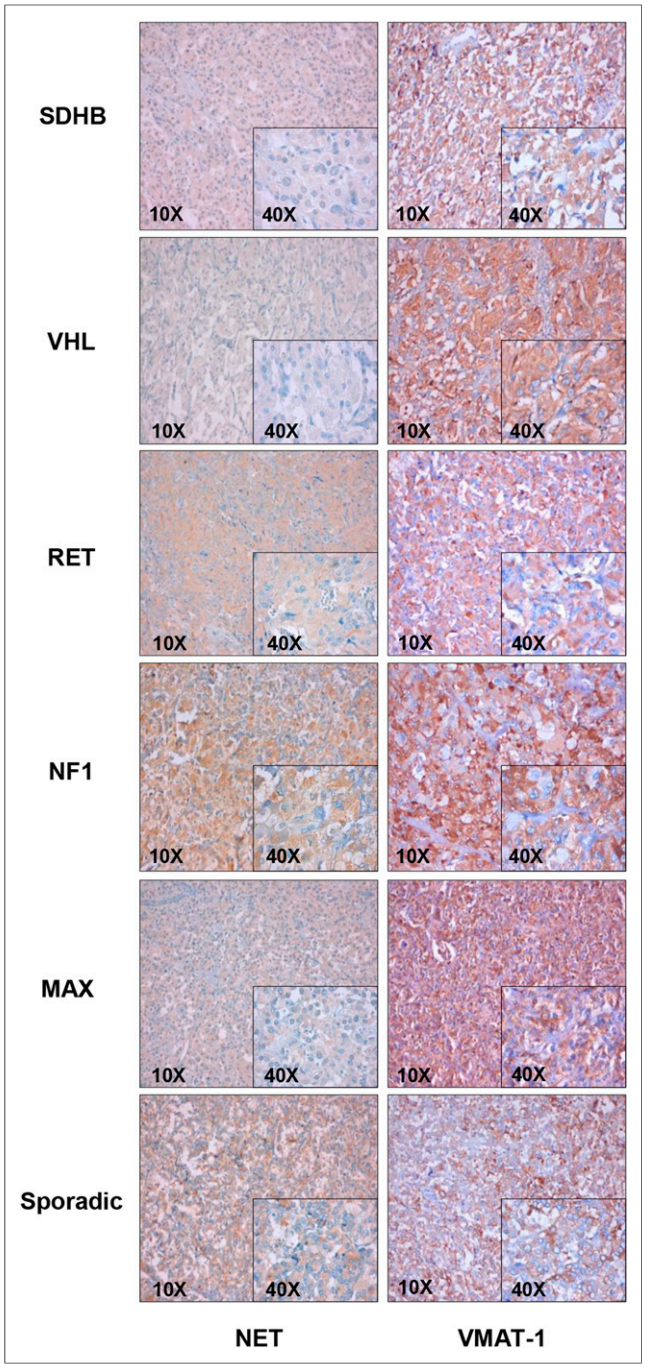

FIGURE 5. Immunohistochemical staining of PPGLs for NET and VMAT-1. Representative images of *SDHD, VHL, RET, NF1, MAX,* and sporadic tumors with magnifications as indicated. Areas with brown (diaminobenzidine polymer) are representative of positive staining.

neurons and sympathetic nerves but is also prominent in chromaffin cells of the adrenal medulla and PPGLs. After entering the cell, similar to norepinephrine, ^{123}I-MIBG translocates from the cytosol into neurosecretory storage vesicles. This process is mediated by VMAT. There are 2 VMAT isoforms, VMAT-1 and VMAT-2, encoded by two different genes and displaying different cellular distributions (*34*). VMAT-1 is mainly expressed in neuroendocrine cells including chromaffin cells, whereas VMAT-2 is expressed in peripheral and central neurons. Fottner et al. have shown that VMAT-1 expression is essential for positive ^{23}I-MIBG scintigraphy of PPGLs (*35*).

Differences in the expression of catecholamine transporters have been reported between *RET*- and *VHL*-related tumors (*36,37*). Huyhn et al. (*36*) showed that *RET*-related PPGLs expressed more NET messenger RNA and protein than *VHL*-related tumors. In contrast, a higher expression of VMAT-1 was found in *VHL*-related tumors, although this was not confirmed at the protein level. Saveanu et al. (*37*) observed a lower NET messenger RNA expression in *VHL*-related PPGLs than sporadic PPGLs, whereas expression of NET in *RET*-related PPGLs was higher. We observed a cytoplasmic staining for NET and VMAT-1 as previously reported by Huyhn et al. (*36*). Our study confirms genotype-dependent differences in the expression of NET and VMAT-1.

The various PPGL genotypes are increasingly recognized as important determinants of functional imaging results. For example, several studies demonstrated a poor overall sensitivity of ^{123}I-MIBG scintigraphy in *SDHB*-related PPGLs (<50%) (*24,25*). Similar to ^{123}I-MIBG, several PET tracers specifically target catecholamine synthesis, storage, and secretion pathways including ^{18}F-fluorodihydroxyphenylalanine and ^{18}F-fluorodopamine. Kaji et al. showed that ^{18}F-fluorodihydroxyphenylalanine PET is superior to ^{123}I-MIBG scintigraphy in the context of von Hippel-Lindau syndrome (*26*). We have previously shown that ^{18}F-FDG PET can distinguish between PPGLs with different underlying genotypes, and sensitivity of ^{18}F-FDG PET is higher in *SDHB/D*-related PPGLs than non–*SDHB/D*-related metastatic PPGLs (92% vs. 37%) (*38*). The sensitivity of ^{123}I-MIBG scintigraphy appears to be lower in *VHL*- and *SDHB*-related PPGLs (*22,25,26*). On the

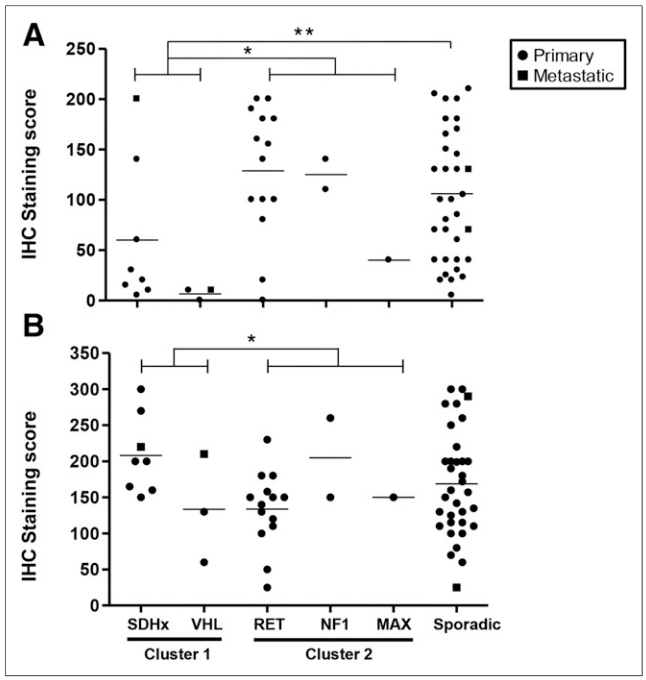

FIGURE 6. Comparison of staining for NET (A) and VMAT-1 (B) among different PPGL genotypes. Graphs represent immunohistochemical staining scores, calculated as percentage area stained positive × staining intensity. Horizontal bar represents mean. Statistical comparisons were performed on the basis of conventional clustering according to predefined transcriptional profiles. *$P < 0.05$, Mann–Whitney *U* test. **$P < 0.01$, Mann–Whitney *U* test.

basis of these studies and the differences in catecholamine transporter expression between genotypes, we hypothesized that a genotype-dependent imaging phenotype also exists for ^{123}I-MIBG scintigraphy. With the current study, we show that this is not the case and that ^{123}I-MIBG uptake appears to be independent of the underlying genotype. Furthermore, we did not find significant correlations between ^{123}I-MIBG uptake and transporter (NET, VMAT-1) expression. On the basis of our results, we argue that, as opposed to certain PET tracers, ^{123}I-MIBG scintigraphy cannot be used for the prediction of underlying genotypes. The observation of relatively low T/L ratios and low NET expression in *VHL* might suggest that ^{123}I-MIBG scintigraphy is of limited use in *VHL*-related PPGLs. This, however, remains to be confirmed in a larger series.

The lack of correlations between ^{123}I-MIBG avidity and NET and VMAT-1 staining might suggest that ^{123}I-MIBG accumulation is not primarily determined by the expression of these transporter systems. However, ^{123}I-MIBG uptake may be determined by NET and VMAT-1 transporter activity rather than transporter quantity. Also, differences in the recruitment of NET from the cytoplasm toward the cell and vesicular membranes may play a role. In addition to transmembrane transport, ^{123}I-MIBG accumulation is also determined by catecholamine storage capacity as reflected by the number of neurosecretory granules (*39*). Other mechanisms besides uptake via NET and VMAT-1 includes passive diffusion, fractional blood content, nonspecific uptake by other transporters, and uptake by nontumor cells such as macrophages and endothelial cells. Another potential explanation for the lack of correlation is the fact that we used the immunohistochemistry staining score in a single tumor tissue section to determine the expression of NET and VMAT-1 in these tumors, which may not be representative of the protein expression of the entire tumor.

Besides genetic factors, we investigated other possible determinants of ^{123}I-MIBG uptake including tumor location, tumor size, and plasma metanephrines concentrations. Several studies have shown that the sensitivity of ^{123}I-MIBG scintigraphy is lower in extraadrenal PPGLs (*33,40*). Saveanu et al. (*37*) reported a higher NET expression in adrenal than extraadrenal PPGLs, which has also been shown to be the case for VMAT-1 expression (*35*). In contrast, we found no differences in NET or VMAT-1 expression between tumor locations and, surprisingly, even a slightly higher ^{123}I-MIBG uptake in extraadrenal PPGL. In addition, we found a significant and positive correlation between maximum tumor diameter and ^{123}I-MIBG uptake regardless of tumor location. This is in line with previous results (*20,23*). MIBG uptake did not correlate with plasma metanephrines. Others also failed to identify any correlation between ^{123}I-MIBG uptake and hormonal levels (*20,33,39*).

This study has several limitations. First, a relatively low number of hereditary PPGLs was available for comparison of genotype-specific ^{123}I-MIBG imaging results. Additional studies with a larger sample size are desired. It would be interesting to also take into account somatic mutations in apparently sporadic PPGLs. Second, semiquantitative T/L ratios may be helpful to distinguish between pathologic and physiologic adrenal uptake but do not necessarily provide a definite answer. There is a considerable overlap between tumors and normal adrenals. The T/L ratio should therefore be merely regarded as an additional aid for the evaluation of MIBG images in the individual clinical context. Third, the use of the left adrenal gland for assessments of physiologic ^{123}I-MIBG uptake in hereditary cases may have some limitations. This adrenal might be affected by adrenal hyperplasia or a subclinical tumor, especially in patients with germline mutations who are at risk for bilateral disease. Although we observed slightly higher NA/L ratios in hereditary PPGLs (data not shown), the ratios largely overlapped with ratios of sporadic PPGLs. This, however, deserves further investigations in a larger study sample.

CONCLUSION

Liver-normalized semiquantitative ^{123}I-MIBG uptake may be helpful to distinguish between pheochromocytoma and physiologic adrenal uptake. The presence of an underlying hereditary syndrome in individual patients cannot be predicted by semiquantitative uptake of ^{123}I-MIBG. Genotype-specific differences in the expression of NET and VMAT-1 do not translate into differences in ^{123}I-MIBG uptake.

DISCLOSURE

The costs of publication of this article were defrayed in part by the payment of page charges. Therefore, and solely to indicate this fact, this article is hereby marked "advertisement" in accordance with 18 USC section 1734. Financial support for this study was provided by the European Union Seventh Framework Program (FP7/2007-2013) under grant agreement no. 259735 (ENSAT CANCER). No other potential conflict of interest relevant to this article was reported.

REFERENCES

1. Leung K, Stamm M, Raja A, Low G. Pheochromocytoma: the range of appearances on ultrasound, CT, MRI, and functional imaging. *AJR.* 2013;200:370–378.
2. Nakajo M, Shapiro B, Copp J, et al. The normal and abnormal distribution of the adrenomedullary imaging agent m-[I-131]iodobenzylguanidine (I-131 MIBG) in man: evaluation by scintigraphy. *J Nucl Med.* 1983;24:672–682.
3. Glowniak JV, Kilty JE, Amara SG, Hoffman BJ, Turner FE. Evaluation of metaiodobenzylguanidine uptake by the norepinephrine, dopamine and serotonin transporters. *J Nucl Med.* 1993;34:1140–1146.
4. van Berkel A, Pacak K, Lenders JW. Should every patient diagnosed with a phaeochromocytoma have a ^{123}I-MIBG scintigraphy? *Clin Endocrinol (Oxf).* 2014;81:329–333.
5. Lenders JW, Duh QY, Eisenhofer G, et al. Pheochromocytoma and paraganglioma: an endocrine society clinical practice guideline. *J Clin Endocrinol Metab.* 2014;99:1915–1942.
6. Lenders JW, Eisenhofer G, Mannelli M, Pacak K. Phaeochromocytoma. *Lancet.* 2005;366:665–675.
7. Gimenez-Roqueplo AP, Dahia PL, Robledo M. An update on the genetics of paraganglioma, pheochromocytoma, and associated hereditary syndromes. *Horm Metab Res.* 2012;44:328–333.
8. Dahia PL. Pheochromocytoma and paraganglioma pathogenesis: learning from genetic heterogeneity. *Nat Rev Cancer.* 2014;14:108–119.
9. López-Jiménez E, Gomez-Lopez G, Leandro-Garcia LJ, et al. Research resource: Transcriptional profiling reveals different pseudohypoxic signatures in SDHB and VHL-related pheochromocytomas. *Mol Endocrinol.* 2010;24:2382–2391.
10. Eisenhofer G, Huynh TT, Pacak K, et al. Distinct gene expression profiles in norepinephrine- and epinephrine-producing hereditary and sporadic pheochromocytomas: activation of hypoxia-driven angiogenic pathways in von Hippel-Lindau syndrome. *Endocr Relat Cancer.* 2004;11:897–911.
11. Liu B, Zhuang H, Servaes S. Comparison of [^{123}I]MIBG and [^{131}I]MIBG for imaging of neuroblastoma and other neural crest tumors. *Q J Nucl Med Mol Imaging.* 2013;57:21–28.
12. Lynn MD, Shapiro B, Sisson JC, et al. Pheochromocytoma and the normal adrenal medulla: improved visualization with I-123 MIBG scintigraphy. *Radiology.* 1985;155:789–792.
13. Sharma P, Dhull VS, Jeph S, et al. Can hybrid SPECT-CT overcome the limitations associated with poor imaging properties of ^{131}I-MIBG? Comparison with planar scintigraphy and SPECT in pheochromocytoma. *Clin Nucl Med.* 2013;38:e346–e353.

14. Timmers HJ, Chen CC, Carrasquillo JA, et al. Comparison of ^{18}F-fluoro-L-DOPA, ^{18}F-fluoro-deoxyglucose, and ^{18}F-fluorodopamine PET and ^{123}I-MIBG scintigraphy in the localization of pheochromocytoma and paraganglioma. *J Clin Endocrinol Metab.* 2009;94:4757–4767.
15. Nakatani T, Hayama T, Uchida J, Nakamura K, Takemoto Y, Sugimura K. Diagnostic localization of extra-adrenal pheochromocytoma: comparison of ^{123}I-MIBG imaging and ^{131}I-MIBG imaging. *Oncol Rep.* 2002;9:1225–1227.
16. Van Der Horst-Schrivers AN, Jager PL, Boezen HM, Schouten JP, Kema IP, Links TP. Iodine-123 metaiodobenzylguanidine scintigraphy in localising phaeochromocytomas–experience and meta-analysis. *Anticancer Res.* 2006;26:1599–1604.
17. Wiseman GA, Pacak K, O'Dorisio MS, et al. Usefulness of ^{123}I-MIBG scintigraphy in the evaluation of patients with known or suspected primary or metastatic pheochromocytoma or paraganglioma: results from a prospective multicenter trial. *J Nucl Med.* 2009;50:1448–1454.
18. Furuta N, Kiyota H, Yoshigoe F, Hasegawa N, Ohishi Y. Diagnosis of pheochromocytoma using [^{123}I]-compared with [^{131}I]-metaiodobenzylguanidine scintigraphy. *Int J Urol.* 1999;6:119–124.
19. Maurea S, Cuocolo A, Imbriaco M, et al. Imaging characterization of benign and malignant pheochromocytoma or paraganglioma: comparison between MIBG uptake and MR signal intensity ratio. *Ann Nucl Med.* 2012;26:670–675.
20. Mozley PD, Kim CK, Moshin J, Gosfield E, Alavi A. The efficacy of iodine-123-MIBG as a screening test for pheochromocytoma. *J Nucl Med.* 1994;35:1138–1144.
21. Timmers HJ, Eisenhofer G, Carrasquillo JA, et al. Use of 6-[^{18}F]-fluorodopamine positron emission tomography (PET) as first-line investigation for the diagnosis and localization of non-metastatic and metastatic phaeochromocytoma (PHEO). *Clin Endocrinol (Oxf).* 2009;71:11–17.
22. Timmers HJ, Kozupa A, Chen CC, et al. Superiority of fluorodeoxyglucose positron emission tomography to other functional imaging techniques in the evaluation of metastatic SDHB-associated pheochromocytoma and paraganglioma. *J Clin Oncol.* 2007;25:2262–2269.
23. van der Harst E, de Herder WW, Bruining HA, et al. [^{123}I]metaiodobenzylguanidine and [^{111}In]octreotide uptake in benign and malignant pheochromocytomas. *J Clin Endocrinol Metab.* 2001;86:685–693.
24. Gimenez-Roqueplo AP, Caumont-Prim A, Houzard C, et al. Imaging work-up for screening of paraganglioma and pheochromocytoma in SDHx mutation carriers: a multicenter prospective study from the PGL.EVA Investigators. *J Clin Endocrinol Metab.* 2013;98:E162–E173.
25. Fonte JS, Robles JF, Chen CC, et al. False-negative ^{123}I-MIBG SPECT is most commonly found in SDHB-related pheochromocytoma or paraganglioma with high frequency to develop metastatic disease. *Endocr Relat Cancer.* 2012;19:83–93.
26. Kaji P, Carrasquillo JA, Linehan WM, et al. The role of 6-[^{18}F]fluorodopamine positron emission tomography in the localization of adrenal pheochromocytoma associated with von Hippel-Lindau syndrome. *Eur J Endocrinol.* 2007;156:483–487.
27. Lenders JW, Eisenhofer G, Armando I, Keiser HR, Goldstein DS, Kopin IJ. Determination of metanephrines in plasma by liquid chromatography with electrochemical detection. *Clin Chem.* 1993;39:97–103.
28. Bombardieri E, Giammarile F, Aktolun C, et al. ^{131}I/^{123}I-metaiodobenzylguanidine (mIBG) scintigraphy: procedure guidelines for tumour imaging. *Eur J Nucl Med Mol Imaging.* 2010;37:2436–2446.
29. Solanki KK, Bomanji J, Moyes J, Mather SJ, Trainer PJ, Britton KE. A pharmacological guide to medicines which interfere with the biodistribution of radiolabelled meta-iodobenzylguanidine (MIBG). *Nucl Med Commun.* 1992;13:513–521.
30. Lee M, Marinoni I, Irmler M, et al. Transcriptome analysis of MENX-associated rat pituitary adenomas identifies novel molecular mechanisms involved in the pathogenesis of human pituitary gonadotroph adenomas. *Acta Neuropathol.* 2013;126:137–150.
31. Bland JM, Altman DG. Statistical methods for assessing agreement between two methods of clinical measurement. *Lancet.* 1986;1:307–310.
32. Cecchin D, Lumachi F, Marzola MC, et al. A meta-iodobenzylguanidine scintigraphic scoring system increases accuracy in the diagnostic management of pheochromocytoma. *Endocr Relat Cancer.* 2006;13:525–533.
33. Bhatia KS, Ismail MM, Sahdev A, et al. ^{123}I-metaiodobenzylguanidine (MIBG) scintigraphy for the detection of adrenal and extra-adrenal phaeochromocytomas: CT and MRI correlation. *Clin Endocrinol (Oxf).* 2008;69:181–188.
34. Erickson JD, Schafer MK, Bonner TI, Eiden LE, Weihe E. Distinct pharmacological properties and distribution in neurons and endocrine cells of two isoforms of the human vesicular monoamine transporter. *Proc Natl Acad Sci USA.* 1996;93:5166–5171.
35. Fottner C, Helisch A, Anlauf M, et al. 6-^{18}F-fluoro-L-dihydroxyphenylalanine positron emission tomography is superior to ^{123}I-metaiodobenzyl-guanidine scintigraphy in the detection of extraadrenal and hereditary pheochromocytomas and paragangliomas: correlation with vesicular monoamine transporter expression. *J Clin Endocrinol Metab.* 2010;95:2800–2810.
36. Huynh TT, Pacak K, Brouwers FM, et al. Different expression of catecholamine transporters in phaeochromocytomas from patients with von Hippel-Lindau syndrome and multiple endocrine neoplasia type 2. *Eur J Endocrinol.* 2005;153:551–563.
37. Saveanu A, Muresan M, De Micco C, et al. Expression of somatostatin receptors, dopamine D_2 receptors, noradrenaline transporters, and vesicular monoamine transporters in 52 pheochromocytomas and paragangliomas. *Endocr Relat Cancer.* 2011;18:287–300.
38. Timmers HJ, Chen CC, Carrasquillo JA, et al. Staging and functional characterization of pheochromocytoma and paraganglioma by ^{18}F-fluorodeoxyglucose (^{18}F-FDG) positron emission tomography. *J Natl Cancer Inst.* 2012;104:700–708.
39. Bomanji J, Levison DA, Flatman WD, et al. Uptake of iodine-123 MIBG by pheochromocytomas, paragangliomas, and neuroblastomas: a histopathological comparison. *J Nucl Med.* 1987;28:973–978.
40. Taieb D, Neumann H, Rubello D, Al-Nahhas A, Guillet B, Hindie E. Modern nuclear imaging for paragangliomas: beyond SPECT. *J Nucl Med.* 2012;53:264–274.